Chapter

Detection of Stator and Rotor Asymmetries Faults in Wound Rotor Induction Machines: Modeling, Test and Real-Time Implementation

Shahin Hedayati Kia

Abstract

This chapter deals with detection of stator and rotor asymmetries faults in wound rotor induction machines using rotor and stator currents signatures analysis. This is proposed as the experimental part of *fault diagnosis in electrical machines* course for master's degree students in electrical engineering at University of Picardie "Jules Verne". The aim is to demonstrate the main steps of real-time condition monitoring development for wound rotor induction machines. In this regard, the related parameters of classical model of wound rotor induction machine under study are initially estimated. Then, the latter model is validated through experiments in both healthy and faulty conditions at different levels of the load. Finally, an algorithm is implemented in a real-time data acquisition system for online detection of stator and rotor asymmetries faults. An experimental test bench based on a three-phase 90 W wound rotor induction machine and a real-time platform for hardware-in-the-loop test are utilized for validation of the proposed condition monitoring techniques.

Keywords: AC motor protection, asynchronous rotating machines, fault diagnosis, Fourier transform, hardware-in-the-loop, induction motors, monitoring, signal processing

1. Introduction

Fault diagnosis of electrical machines is a very active topic of research and several books have been published, which detail new developed techniques for efficient condition monitoring of electrical machines. The run-to-break is an unplanned strategy of maintenance that needs to be avoided at the expense of high emergency repair cost. By means of preventive maintenance at regular intervals, which is commonly shorter than the expected time between failures, the maintenance actions can be planned in advance. Any potential breakdown in industrial systems can be predicted through the condition based maintenance (CBM) so called 'predictive maintenance' which gives a reasonable remaining useful life and leads consequently to the optimum time maintenance planning [1]. Since the electrical machines are the key components of the majority of industrial processes, it is essential to setup a CBM in order to minimize their downtime and consequently

increase their availability [2, 3]. Modeling and numerical simulations are the initial design stage of fault detection and diagnosis (FDD) systems [4]. For prototyping and testing both software-in-the-loop (S-i-L) and hardware-in-the-loop (H-i-L) realizations can be performed before the final stage of FDD system integration [4]. This leads to a better evaluation of FDD methods in all possible working condition scenarios which are sometimes hard to acquire in real practice using an experimental test bench. In this chapter, the illustration of these previous stages to Masters' degree students who attend to assimilate the ability of FDD technique development for electrical systems will be highlighted. The example of wound rotor induction machine (WRIM) is a good choice since WRIMs have been widely used in electrical power generation, particularly as doubly fed induction generators (DFIGs) in variable speed wind turbines. Moreover, the internal circuit parameters of a WRIM can be easily deduced using some basic experimental electrical circuit tests. The asymmetry fault in practice can be obtained by adding series resistance in one phase of stator and/or rotor winding which simplifies the evaluation of FDD methods through both numerical simulations and experiments. The state-of-the-art methods for FDD of asymmetries in WRIMs have been well detailed [5]. However, the implementation of FDD algorithms in real-time systems has been rarely investigated [6]. Recently, the H-i-L configuration is used for static eccentricity analysis in induction machines (IMs). However, the proposed model is exclusively validated using finite elements method (FEM). The real-time simulation results have been demonstrated the presence of fault-related frequency components in the stator current spectrum [3]. In this regard, introducing engineering students to FDD system design for electrical machines including its development stages is totally new in the literature [7–9]. The aim of this paper is to illustrate the main stages of FDD system design for the stator asymmetry fault (SAF) as well as the rotor asymmetry fault (RAF) in WRIMs. This is proposed as the experimental part of *fault diagnosis in electrical machines* course offered to the master's degree students in electrical engineering at University of Picardie "Jules Verne". Both stator and rotor windings asymmetries are investigated. Main emphasis is dedicated to signal-based techniques which are commonly used for detection of these specific defects. It is illustrated that the stator current is directly affected by the RAF whereas the SAF has a direct influence on the rotor current [5]. The fault diagnosis is commonly performed by computing the stator/rotor current Fourier transform to identify the fault-related frequency components in the spectrum in steady-state working condition. Once the validated WRIM model is implemented in a real-time platform for H-i-L test, the measured stator and rotor currents signals, provided by the real-time system, can be analyzed by the CompactRIO data acquisition system for evaluation of signal processing tools (SPTs) in all working condition scenarios of WRIM. An experimental test bench, based on a three-phase 90 W wound rotor induction machine and a real-time platform for H-i-L tests, are utilized for validation of the proposed condition monitoring techniques.

2. Modeling of WRIM

The model of WRIM in "*abc*" reference frame may be expressed as [10]:

$$\mathbf{v}_{abcs} = \mathbf{r}_s \mathbf{i}_{abcs} + \frac{d}{dt}\boldsymbol{\lambda}_{abcs} \tag{1}$$

$$\mathbf{v}_{abcr} = \mathbf{r}_r \mathbf{i}_{abcr} + \frac{d}{dt}\boldsymbol{\lambda}_{abcr} \tag{2}$$

$$\begin{bmatrix} \boldsymbol{\lambda}_{abcs} \\ \boldsymbol{\lambda}_{abcr} \end{bmatrix} = \begin{bmatrix} \mathbf{L}_s & \mathbf{L}_{sr} \\ \mathbf{L}_{sr}^T & \mathbf{L}_r \end{bmatrix} \begin{bmatrix} \mathbf{i}_{abcs} \\ \mathbf{i}_{abcr} \end{bmatrix} \tag{3}$$

$$\mathbf{r}_s = \begin{bmatrix} r_{as} & 0 & 0 \\ 0 & r_{bs} & 0 \\ 0 & 0 & r_{cs} \end{bmatrix} \tag{4}$$

$$\mathbf{r}_r = \begin{bmatrix} r_{ar} & 0 & 0 \\ 0 & r_{br} & 0 \\ 0 & 0 & r_{cr} \end{bmatrix} \tag{5}$$

$$\mathbf{L}_s = \begin{bmatrix} L_{ls} + L_{ms} & -\frac{1}{2}L_{ms} & -\frac{1}{2}L_{ms} \\ -\frac{1}{2}L_{ms} & L_{ls} + L_{ms} & -\frac{1}{2}L_{ms} \\ -\frac{1}{2}L_{ms} & -\frac{1}{2}L_{ms} & L_{ls} + L_{ms} \end{bmatrix} \tag{6}$$

$$\mathbf{L}_r = \begin{bmatrix} L_{lr} + L_{mr} & -\frac{1}{2}L_{mrs} & -\frac{1}{2}L_{mr} \\ -\frac{1}{2}L_{mr} & L_{ls} + L_{mr} & -\frac{1}{2}L_{mr} \\ -\frac{1}{2}L_{mr} & -\frac{1}{2}L_{mr} & L_{lr} + L_{mr} \end{bmatrix} \tag{7}$$

$$\mathbf{L}_{sr} = L_{sr} \times \begin{bmatrix} cos\,(\theta_r) & cos\,(\theta_r + 2\pi/3) & cos\,(\theta_r - 2\pi/3) \\ cos\,(\theta_r - 2\pi/3) & cos\,(\theta_r) & cos\,(\theta_r + 2\pi/3) \\ cos\,(\theta_r + 2\pi/3) & cos\,(\theta_r - 2\pi/3) & cos\,(\theta_r) \end{bmatrix} \tag{8}$$

$$\begin{aligned} T_e = {} & i_{as}L_{sr}\{-i_{ar}\,sin\,(\theta_r) - i_{br}\,sin\,(\theta_r + 2\pi/3) \\ & -i_{cr}\,sin\,(\theta_r - 2\pi/3)\} \times p + \\ & i_{bs}L_{sr}\{-i_{ar}\,sin\,(\theta_r - 2\pi/3) - i_{br}\,sin\,(\theta_r) \\ & -i_{cr}\,sin\,(\theta_r + 2\pi/3)\} \times p + \\ & i_{cs}L_{sr}\{-i_{ar}\,sin\,(\theta_r + 2\pi/3) - i_{br}\,sin\,(\theta_r - 2\pi/3) \\ & -i_{cr}\,sin\,(\theta_r)\} \times p \end{aligned} \tag{9}$$

$$T_e - T_l = J\frac{d\Omega_r}{dt} + f\Omega_r \tag{10}$$

with

$$\Omega_r = 2 \times \pi \times \ p \times \frac{d\theta_r}{dt} \tag{11}$$

where L_{ms}, L_{mr}, L_{ls} and L_{lr} are magnetizing and leakage stator and rotor inductances and r_{as}, r_{bs}, r_{cs}, r_{ar}, r_{br} and r_{cr} are stator and rotor phase resistances respectively. T_e is the electromagnetic torque, T_l is the load torque, J is the total moment inertia, f is the viscous friction coefficient, p is the number of pole pairs, and θ_r is the rotor angular speed. The estimation of WRIM model parameters, described by relations (1) and (2), is straightforward and can be performed through some basic electrical circuit tests. DC voltage–current experiments at rated working

temperature of WRIM give an initial estimation of both stator phase resistances r_{as}, r_{bs}, and r_{cs} ($r_{as} \approx r_{bs} \approx r_{cs}$) and rotor phase resistances r_{ar}, r_{br} and r_{cr} ($r_{ar} \approx r_{br} \approx r_{cr}$) respectively. The obtained values are commonly good enough for arranging the model and for studing the asymmetry fault in WRIMs. Knowing these previous resistances, the respective stator-related self-inductances i.e. $L_{as} \approx L_{bs} \approx L_{cs} = L_{ms} + L_{ls}$ and mutual inductances i.e. $L_{abs} \approx L_{acs} \approx L_{bcs} = -0.5 \times L_{ms}$ can be obtained according to the relations (12)–(15). An AC voltage source is necessary for providing rated voltages to the stator phase windings as it is depicted in **Figure 1**.

$$L_{as} = \sqrt{\frac{\left(\frac{V_{as}}{I_{as}}\right)^2 - r_{as}^2}{\omega_s^2}} \tag{12}$$

$$L_{cs} \approx L_{bs} \approx L_{as} \tag{13}$$

$$L_{abs} = \frac{V_{bs}}{I_{as}\omega_s} \tag{14}$$

$$L_{bcs} \approx L_{acs} \approx L_{abs} \tag{15}$$

Similarly, the respective rotor-related self-inductances i.e. $L_{ar} \approx L_{br} \approx L_{cr} = L_{mr} + L_{lr}$ and mutual inductances i.e. $L_{abr} \approx L_{acr} \approx L_{bcr} = -0.5 \times L_{mr}$ can be evaluated according to the relations (16)–(19).

$$L_{ar} = \sqrt{\frac{\left(\frac{V_{ar}}{I_{ar}}\right)^2 - r_{ar}^2}{\omega_s^2}} \tag{16}$$

$$L_{cr} \approx L_{br} \approx L_{ar} \tag{17}$$

$$L_{abr} = \frac{V_{br}}{I_{ar}\omega_s} \tag{18}$$

$$L_{bcr} \approx L_{acr} \approx L_{abr} \tag{19}$$

The stator-rotor mutual inductance L_{sr} can be determined using (20).

$$L_{sr} = \frac{V_{ar-max}}{I_{as}\omega_s} \tag{20}$$

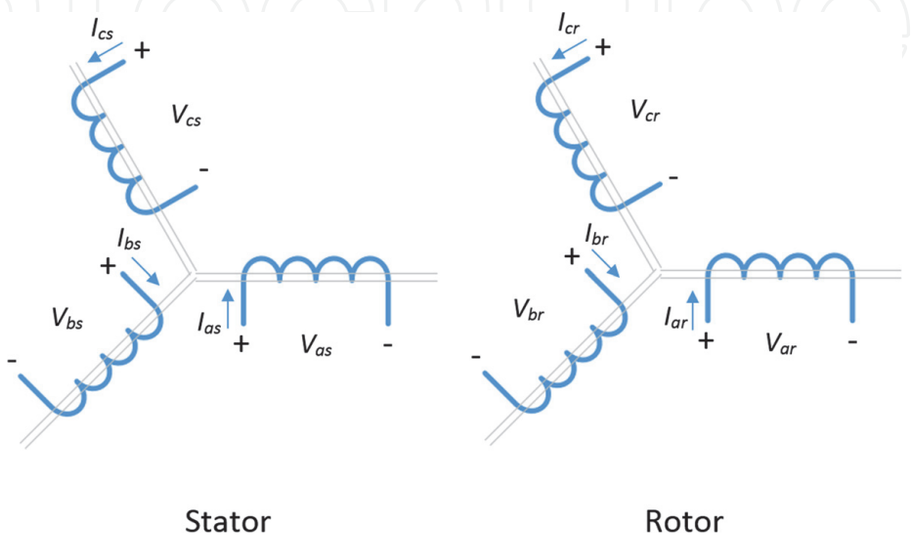

Figure 1.
Scheme of experiments for estimation of WRIM 'abc' reference frame model parameters.

where V_{ar-max} is the voltage peak value obtained across one phase of the rotor winding when the stator is supplied by a voltage source and its current is I_{as}.

3. Healthy working condition

For development of FDD techniques, it is crucial to validate experimentally the proposed model of WRIM in healthy working condition at different levels of the load in both time and frequency domains. Accordingly, the parameters of "*abc*" reference frame model for a WRIM with electrical characteristics, shown in **Table 1**, are estimated using (12)–(20) and listed in **Table 2**. **Figure 2** illustrates the realization of the model in Matlab/Simulink software using trapezoidal integration

Power	90 W
Voltage	380 V
Stator current	0.27 A
Rotor speed	1430 rpm
Pole pairs	2
Torque	0.6 N.m
Rotor inertia	0.001 Kg.m^2

Table 1.
Electrical and mechanical characteristics of three-phase 90W WRIM.

R_s	79.13 Ω
R_r	3.69 Ω
L_s	2.82 H
L_r	0.23 H
L_{ms}	2.20 H
L_{mr}	0.22 H
L_{sr}	0.67 H

Table 2.
Estimated parameters of three-phase 90W WRIM "abc" reference frame model.

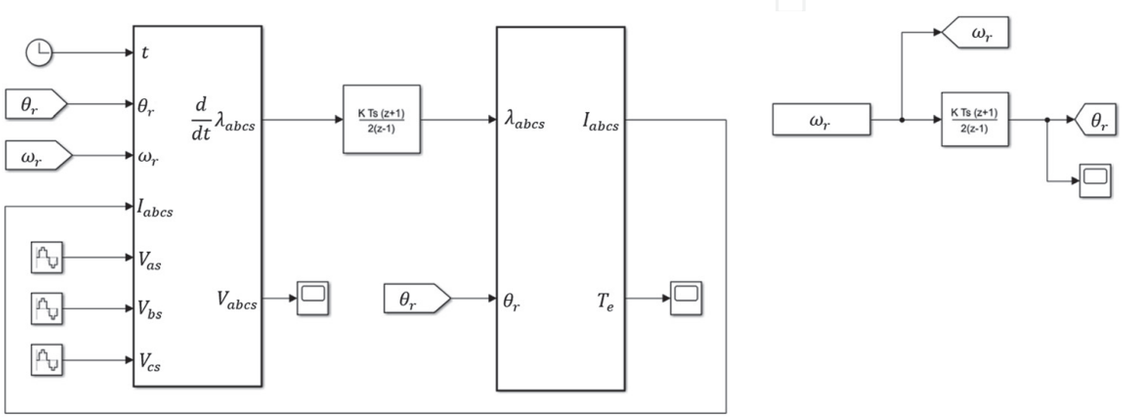

Figure 2.
Realization of WRIM "abc" reference frame model in Matlab/Simulink.

method. Two discrete-time integrators which are closely linked to the relations (1), (2) and (11) are utilized. The model is initially validated through experiment in time domain at different levels of the load. **Figure 3** depicts the results of numerical simulation and experiment at rated load of WRIM. This simple approach gives a general idea of WRIM modeling to the students who are not familiar with this technique. Besides, it is helpful at this stage to localize the main frequency components in both stator and rotor phase currents spectra. f_s is the main frequency component in the stator phase current spectrum whereas f_{Ir} is the main frequency component in the rotor phase current spectrum.

$$f_{Ir} = f_s - p\frac{\Omega_r}{60} \tag{21}$$

where p is the pole pairs and Ω_r is the rotor mechanical speed. The stator and rotor currents spectra of numerical simulation and experiment at rated slip $s_r = 0.047$ are shown in **Figure 4**. The rotor and stator asymmetries can be performed simply by including an additional series resistance in one of the rotor and stator phases. This technique is the simplest way to familiarize students with fault detection methods in WRIMs which will be highlighted in next sections.

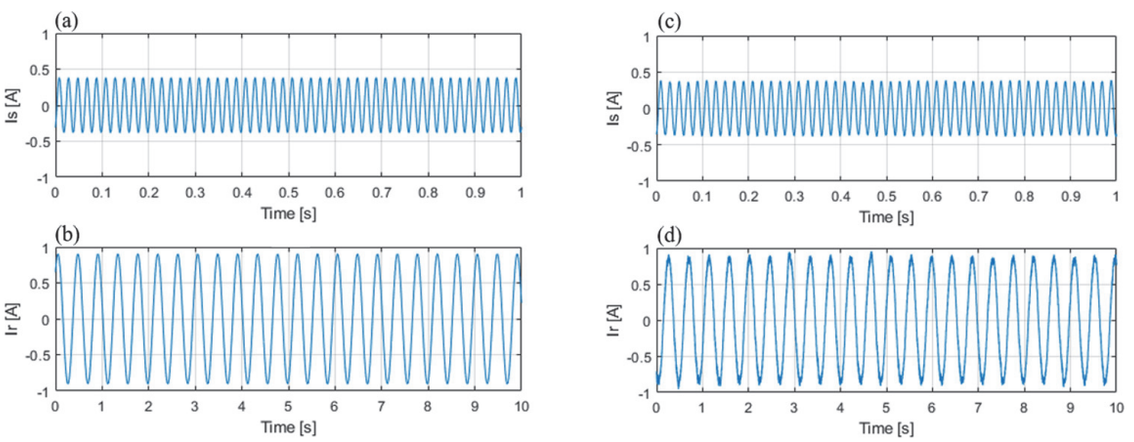

Figure 3.
Healthy condition stator and rotor phase currents of WRIM in time domain (a), (b) numerical simulation (c), (d) experiment.

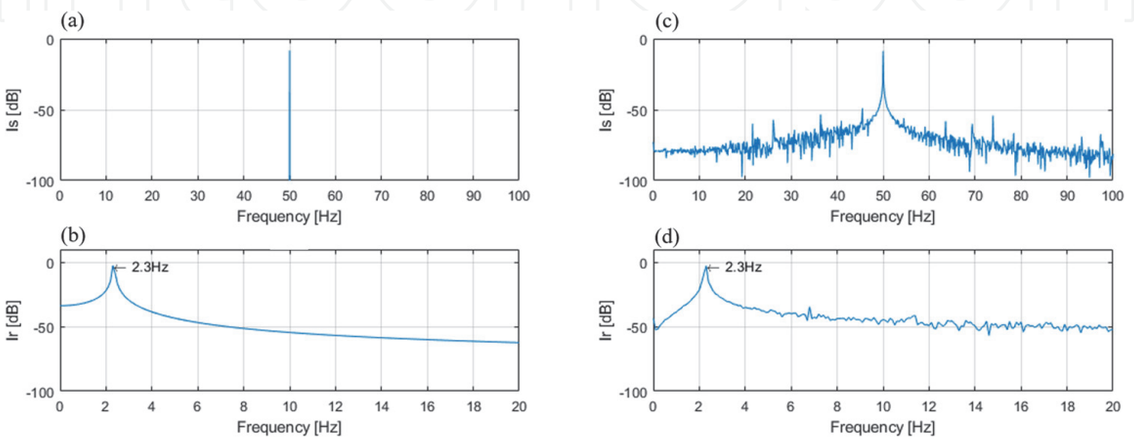

Figure 4.
Healthy condition stator and rotor phase currents of WRIM in frequency domain (a), (b) numerical simulation (c), (d) experiment.

4. RAF detection

It is well known that any deviation from the normal operation of WRIM, resulted from an internal or external anomalies, may induce fault signatures in the electrical variables such as stator and rotor currents. It was illustrated that the stator current is directly affected by the RAF whereas the SAF has a direct influence on the rotor current [5, 11]. The fault diagnosis is commonly carried out by computing the stator/rotor current Fourier transform to locate fault frequency components in the spectrum. An addition resistance $R_{RAF} = 1\Omega$ is included in one of the rotor phases to create the RAF. **Figure 5** illustrates the numerical simulation and experimental results of the stator and rotor phase currents in time domain. As it can be observed, it is quite difficult to detect the RAF through time domain analysis, particularly for small values of R_{RAF}. If the rotor speed of WRIM is considered constant, the following unique frequency component will appear in the stator phase current spectrum [12]:

$$f_{RAF} = (1 - 2s)f_s \tag{22}$$

where s is the slip value. The RAF frequency-related component is well localized in both numerical simulation and experiment spectra of the stator phase current at rated slip value of WRIM (**Figure 6**). Furthermore, the fact that the stator phase current is directly affected by the RAF is well depicted in this last figure.

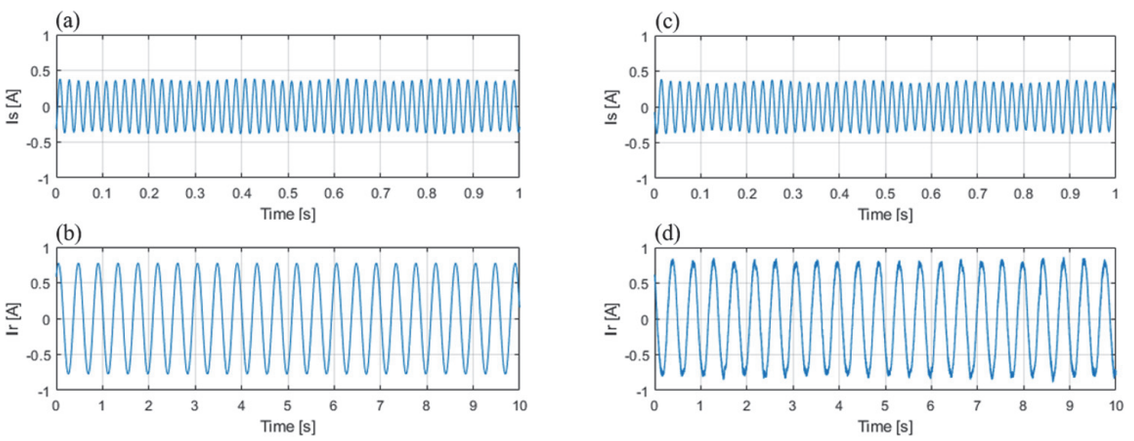

Figure 5.
RAF condition stator and rotor phase currents of WRIM in time domain (a), (b) numerical simulation (c), (d) experiment.

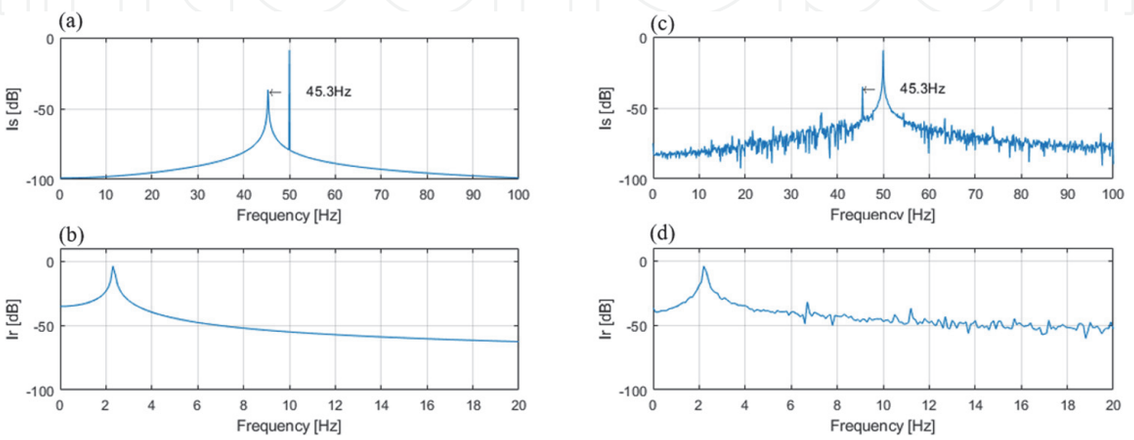

Figure 6.
RAF condition stator and rotor phase currents of WRIM in frequency domain (a), (b) numerical simulation (c), (d) experiment.

5. SAF detection

The frequency components in the rotor phase currents due to the SAF can be obtained as [13]:

$$f_{SAF,k'} = \left\{\frac{k'}{p}(1-s) \pm 1\right\} f_s \tag{23}$$

where $k' = 1, 2, 3, \ldots$. Taking only the fundamental frequency component into account with $\frac{k'}{p} = 1$, the relation (23) can be written as

$$f_{SAF} = (2-s) f_s \tag{24}$$

An additional series resistance $R_{SAF} = 10\Omega$ is included in one of the stator phases to create the SAF. **Figure 7** illustrates the numerical simulation and experimental results of the stator and rotor phase currents at rated slip value of WRIM in time domain.

The SAF frequency-related component is well localized in both numerical simulation and experiment spectra of the rotor phase current at rated load of WRIM (**Figure 8**). Besides, it is well illustrated in **Figure 8**, where the rotor phase current is directly affected by the SAF [11].

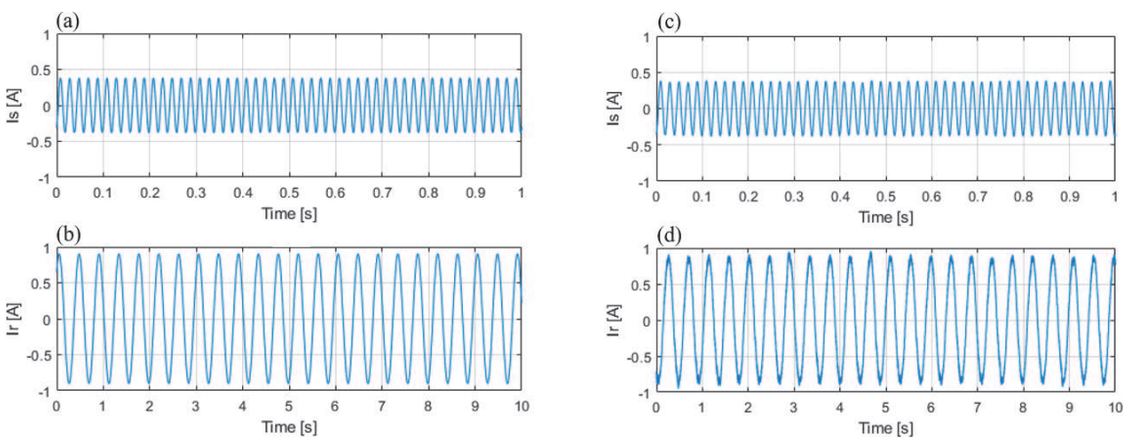

Figure 7.
SAF condition stator and rotor phase currents of WRIM in time domain (a), (b) numerical simulation (c), (d) experiment.

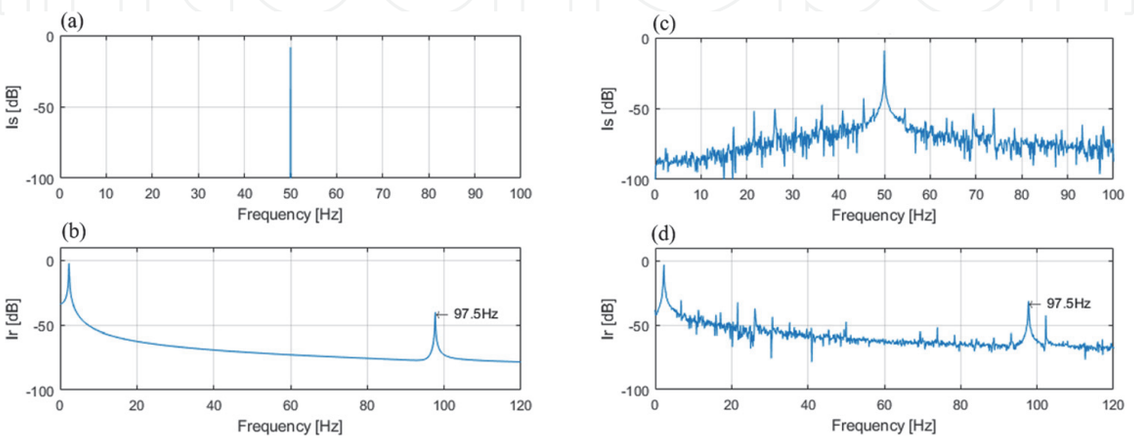

Figure 8.
SAF condition stator and rotor phase currents of WRIM in frequency domain (a), (b) numerical simulation (c), (d) experiment.

6. Real-time RAF and SAF detections

The utilization of SPTs is the crucial stage of the RAF and the SAF detections in both steady-state and transient working conditions of WRIM. The developed methods can be classified in time, frequency and time-frequency/time-scale domains [2]. A brief review of the recent SPTs was mentioned in this topic of research [5]. Up to now, various experimental setups have been designed to evaluate the effectiveness of each SPT. They are mainly defined based upon the rated power of the installed electrical machine in the system. Furthermore, fault detection algorithms are commonly evaluated offline, whereas the new trends are mainly relied on the real-time FDD of electrical machines [6]. The concept of H-i-L is perfectly matched with such a development which is rarely studied [3]. In this regard, a real-time data acquisition system (CompactRIO data acquisition system) is used as a H-i-L with a high performance multi-core real-time platform in order to analyze the performance of different kinds of SPTs in practical conditions (**Figure 9**).

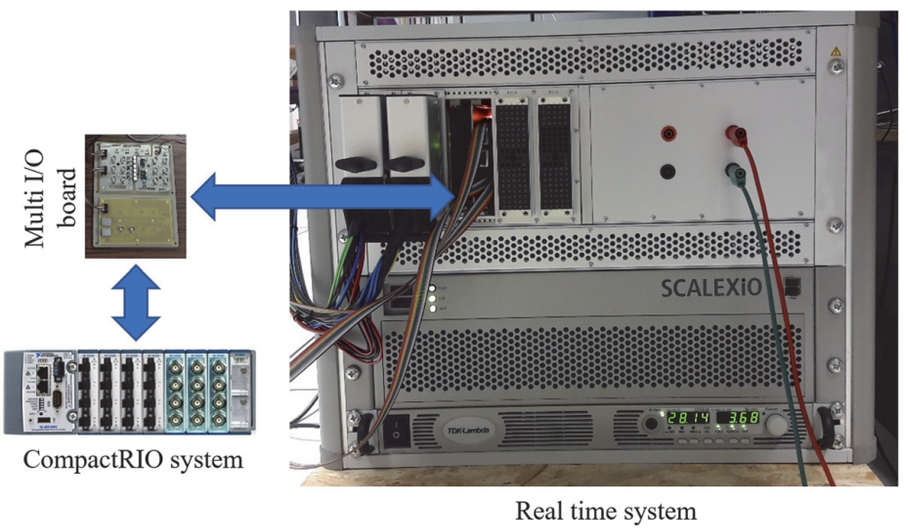

Figure 9.
Configuration of H-i-L test bench.

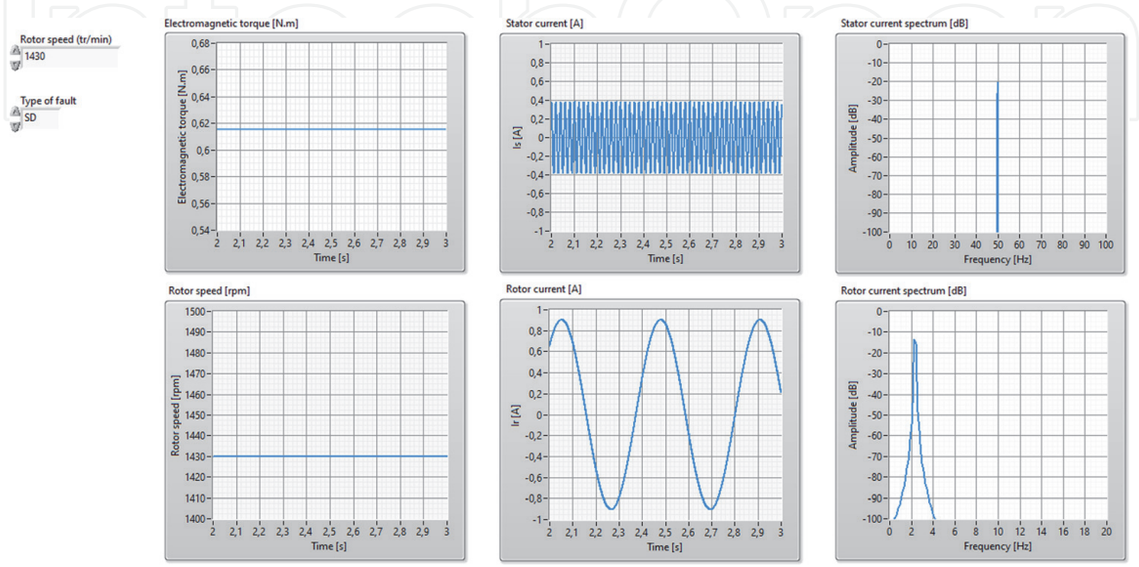

Figure 10.
Healthy condition H-i-L experimental results at rated load of WRIM.

This configuration is particularly attractive as it is totally independent of the type of the under study electrical machine and can be extended to any kind of fault for which an adapted model is well designed. Furthermore, there are more facilities to access the signatures which are commonly difficult to obtain without including high performance sensors in an experimental traditional test bench. The model of WRIM in "*abc*" reference frame, shown in **Figure 2**, is implemented in the real-time system with sampling time $T_s = 10^{-4}$. The stator and rotor current signals, provided by multi I/O board of real-time system, are measured and analyzed by the CompactRIO data acquisition system at 5 kHz sampling frequency for 10s to detect the RAF and the SAF in steady-state working condition of WRIM.

The results of the analysis are illustrated in **Figures 10–12** for the healthy, the RAF and the SAF conditions respectively. The stator and the rotor currents in healthy condition at rated load of WRIM in both time and frequency domains are shown in **Figure 10**. As it would be expected, the main frequency components which are well identified in the spectra are f_s and f_{Ir} respectively. The fault-related

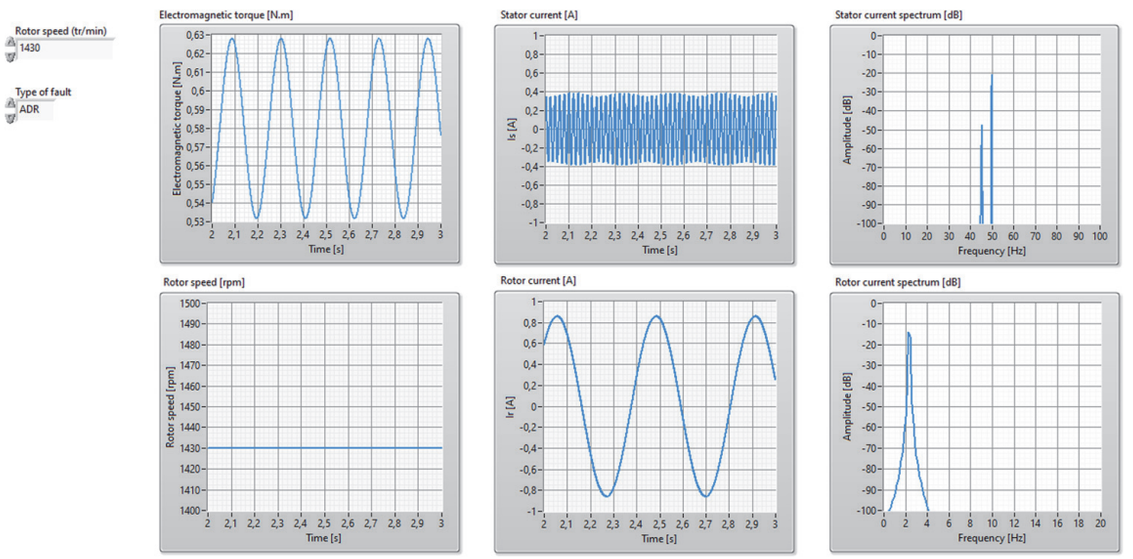

Figure 11.
RAF condition H-i-L experimental results at rated load of WRIM.

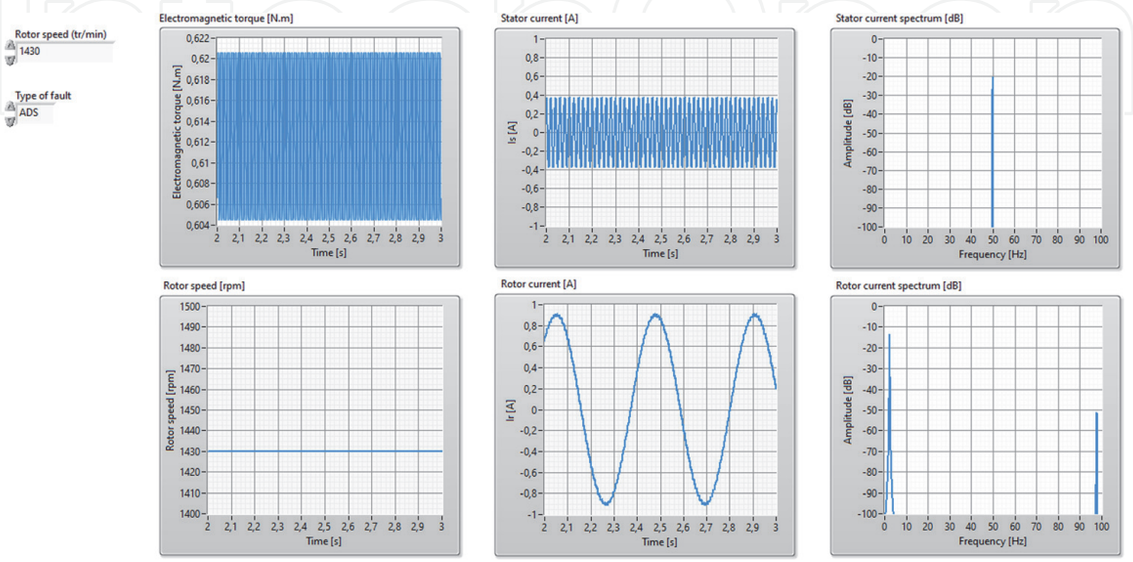

Figure 12.
SAF condition H-i-L experimental results at rated load of WRIM.

frequency component $(1-2s_r)f_s$ ($s_r = 0.047$) is detected in the stator phase current spectrum at rated rotor speed of WRIM (**Figure 11**). The SAF reveals $(2-s_r)f_s$ frequency component in the rotor phase current spectrum as it is shown in **Figure 12**. Besides, the electromagnetic torque is a good indicator of both the RAF and the SAF and can be used as an alternative signature for FDD design (**Figures 11** and **12**).

7. Conclusion

This chapter presents for the first time the concept of H-i-L for fault diagnosis of WRIMs as a part of fault diagnosis of electrical machines course for master's degree students at University of Picardie "Jules Verne". The parameter of WRIM model in "*abc*" reference frame is estimated and validated through experiment at different levels of the load. The developed model is then implemented in a real-time system which is in the loop with a CompactRIO data acquisition platform. This configuration allows to evaluate the SPTs for real-time FDD design in all working conditions of WRIMs. Furthermore, this concept can be extended to condition monitoring of any complex electromechanical system at development stage design.

Abbreviations

RAF	Rotor asymmetry fault
SAF	Stator asymmetry fault
WRIM	Wound rotor induction machine
IM	Induction machine
DFIG	Doubly fed induction generator
FDD	Fault detection and diagnosis
CBM	Condition based maintenance
SPT	Signal processing tool
FEM	Finite element method
S-i-L	Software-in-the-loop
H-i-L	Hardware-in-the-loop

Author details

Shahin Hedayati Kia
MIS Lab. (EA4290), University of Picardie "Jules Verne", Amiens, France

*Address all correspondence to: shdkia@u-picardie.fr

References

[1] Randall RB. Vibration-Based Condition Monitoring: Industrial, Aerospace and Automotive Applications. Wiley; 2011.

[2] Frosini L. Monitoring and diagnostics of electrical machines and drives: A state of the art. In: 2019 IEEE workshop on electrical machines design, Control and Diagnosis (WEMDCD). vol. 1; 2019. p. 169–176.

[3] Sapena-Bano A, Riera-Guasp M, Martinez-Roman J, Pineda-Sanchez M, Puche-Panadero R, Perez-Cruz J. FEM-analytical hybrid model for real time simulation of IMs under static eccentricity fault. In: 2019 IEEE 12th International Symposium on Diagnostics for Electrical Machines, Power Electronics and Drives (SDEMPED); 2019. p. 108–114.

[4] Isermann R. Fault diagnosis systems an introduction from fault detection to fault tolerance. SERBIULA (sistema Librum 20). 2006 01.

[5] Kia SH. Monitoring of wound rotor induction machines by means of discrete wavelet transform. Electric Power Components and Systems. 2018; 46(19–20):2021–2035.

[6] Monmasson E, Idkhajine L, Cirstea MN, Bahri I, Tisan A, Naouar MW. FPGAs in industrial control applications. IEEE Transactions on Industrial Informatics. 2011;7(2): 224–243.

[7] Gómez-de-Gabriel JM, Mandow A, Fernández-Lozano J, García-Cerezo A. Mobile robot lab project to introduce engineering students to fault diagnosis in mechatronic systems. IEEE Transactions on Education. 2015 Aug;58(3):187–193.

[8] Record P. Teaching the art of fault diagnosis in electronics by a virtual learning environment. IEEE Transactions on Education. 2005 Aug; 48(3):375–381.

[9] Pagiatakis G, Dritsas L, Chatzarakis G, Todorov G, Stoev B. Introducing concepts and methodologies of fault detection into electrical engineering education: The induction machine example. In: 2017 IEEE Global Engineering Education Conference (EDUCON); 2017. p. 381–388.

[10] Krause P, Wasynczuk O, Sudhoff SD, Pekarek S. In: Induction motor drives. IEEE; 2013. Available from: https://ieeexplore.ieee.org/document/6739387.

[11] Penman J, Sedding HG, Lloyd BA, Fink WT. Detection and location of interturn short circuits in the stator windings of operating motors. IEEE Transactions on Energy Conversion. 1994;9(4):652–658.

[12] Filippetti F, Franceschini G, Tassoni C, Vas P. AI techniques in induction machines diagnosis including the speed ripple effect. IEEE Transactions on Industry Applications. 1998;34(1):98–108.

[13] Shah D, Nandi S, Neti P. Stator inter-turn fault detection of doubly-fed induction generators using rotor current and search coil voltage signature analysis. In: 2007 IEEE Industry Applications Annual Meeting; 2007. p. 1948–1953.